Journal of Radioanalytical and Nuclear Chemistry
https://doi.org/10.1007/s10967-025-10335-4

Reactivity and volatility of astatine in a quartz column

D. Dietzel[1,2,3] · A. Yakushev[2] · Ch. E. Düllmann[1,2,3] · K. Hermainski[1,2] · J. Ballof[2] · P. Bartl[4] · R. Cantemir[2] · J. John[4] · J. Krier[2] · P. Mošat[2] · M. Němec[4] · J. P. Omtvedt[5] · J. Štursa[6]

Received: 22 May 2025 / Accepted: 6 August 2025

Abstract
Astatine (At, Z = 85) is the rarest naturally occurring element and exhibits unique chemical properties influenced by relativistic effects. The short half-lives of its isotopes and its scarcity limits chemical experiments and methods to study and work with astatine. While some insight has been gained into its behavior in the liquid phase, substantial experimental challenges persist, and studies of its gas-phase chemistry remain scarce. Understanding its reactivity and volatility is important not only for optimizing the use of At in targeted alpha therapy but also a crucial step towards future investigations of its superheavy homolog, tennessine (Ts, Z = 117). Adsorption and interaction of At with a quartz surface were studied aiming at a conclusive understanding of the interaction strength between At and fused silica surfaces of different reactivity. In our work, the isotopes ^{207,208}At ($T_{1/2}$ = 1.63 h and $T_{1/2}$ = 1.81 h, respectively) were produced via fusion-evaporation reactions by irradiating Bi_2O_3-targets with ^{3}He beams. We used gas–solid thermochromatography in various gas atmospheres and applied several temperature gradients ranging from T_{max} = 1000 °C to T_{min} = − 170 °C. Silica surfaces with different degrees of hydroxylation were used. These experiments reveal the concentration of the hydroxyl groups on the surface, i.e. its reactivity, to play an important role in the chemical interaction of At with hot quartz surfaces. Advanced Monte Carlo simulations allowed determining the adsorption enthalpies of the At species, and thus, to elucidate the chemical interactions of At with quartz surfaces. The use of different carrier gases as well as surfaces of different reactivity allowed the production and observation of multiple chemical species. We assigned the most volatile species to elemental At, which was found to be chemically bound to the hydroxylated silica surface at temperatures between 300 and 500 °C.

Keywords Homologs of superheavy elements · Adsorption studies · Astatine · Gas phase chromatography · Monte Carlo simulation · Activated chemisorption

Introduction

Astatine (At), discovered in 1940, is the rarest naturally occurring element on Earth and stands apart from other elements with its extraordinary scarcity and distinct properties [1–4]. All isotopes are short-lived with the most stable isotope being ^{210}At with a half-life of $T_{1/2}$ = 8.1 h. Astatine is primarily produced by irradiating ^{209}Bi targets with alpha-particles. Following the production, elemental At is evaporated from the Bi-targets and distilled in various gases or under vacuum conditions [5, 6]. The dissolution of irradiated targets in HNO_3 with following wet chemistry purification provides another method for At extraction [7]. Due to its ideal decay properties, ^{211}At is one of the best candidates for targeted alpha therapy [8–11]. Several Phase 1 clinical studies have been initiated in the past and are currently ongoing and additional studies are planned for the future [12]. Main challenges on the road to routine clinical use of ^{211}At include its production and handling, and its short half-life. Also the stability of ^{211}At-radioconjugates against in vivo deastatination remains a key point for the application in targeted alpha therapy. Despite being classified as a halogen and its wide

✉ D. Dietzel
dietzel@uni-mainz.de

1 Department of Chemistry, Johannes Gutenberg University Mainz, Mainz, Germany

2 GSI Helmholtzzentrum für Schwerionenforschung, Darmstadt, Germany

3 Helmholtz Institute Mainz, Mainz, Germany

4 Czech Technical University, Prague, Czech Republic

5 University of Oslo, Oslo, Norway

6 Nuclear Physics Institute CAS, Řež, Czech Republic

Published online: 24 September 2025

use similar to iodine in organic synthesis, At exhibits metalloid behavior due to the influence of relativistic effects on its electronic structure, as inferred from theoretical calculations and measurements of the ionization potential and electron affinity [13–17]. While significant progress has been made in understanding the behavior of At in its liquid phase [18, 19], particularly in organic phase for radiopharmaceutical applications, its gas-phase interactions remain areas of active exploration [20–23]. Gas chromatography is known for its efficiency in studying the interactions of single, short-lived atoms with a stationary phase, and has been used in previous studies involving superheavy elements and their lighter homologs [24–26]. As a lighter homolog of the superheavy element tennessine (Ts, Z = 117), At also plays a crucial role in planning future superheavy element experiments. With moscovium (Mc, Z = 115) being the heaviest element chemically studied [27], technical developments progress toward even heavier nuclei. In the coming years, experiments with Ts will come into focus, despite the short half-life of even the most long-lived currently known isotope, ^{294}Ts ($T_{1/2} = 51^{+38}_{-16}$ ms [28]) and low production rate. Technical developments will enable rapid and efficient extraction into chemistry setups, bringing livermorium (Lv, Z = 116) as well as Ts within reach of chemical investigation [29, 30]. This advancement also underscores the importance of studying the gas-phase chemistry of At to facilitate future experiments with Ts and to provide a basis for comparison. In contrast to homologs of Fl and Mc, namely Pb and Bi, macroscopic amounts for superheavy element homologs heavier than Bi do not exist, forcing researchers to use radiochemical methods to study the behavior of At and its compounds. It is crucial to note the strong interactions of elements from Hg to At with Au surfaces due to their metallic or semi-metallic nature [31–37], while quartz surfaces, which are generally less reactive, enable effective separation of elements and compounds during experiments. The known experimentally determined adsorption enthalpies of the 6p and 7p elements are summarized in Table 1.

Based on theoretical calculations [45, 46], as well as experiments listed in Table 1, no separation of the elements Hg, Tl, Pb, Bi, Mc, Po and At would be possible on Au surfaces at ambient temperature. All elements interact strongly enough with Au surfaces at room temperature for immediate immobilization, rather than multiple adsorption–desorption steps. For their separation, temperatures well above room temperature are needed. Since the positional detection inside the column is realized by capturing the alpha-decays with PIN diode detectors, which form the gas chromatography channel, the temperature is limited by the operating temperature range of the PIN diodes. In contrast, less reactive quartz surfaces have been successfully utilized in separating and characterizing superheavy elements such copernicium (Cn, Z = 112) [38], Nh [27, 47, 48], Fl [42], and Mc [27] in addition to Au surfaces, even at low temperatures. While the surface structure of Au is well defined in theoretical models (less so in real experiments [42]), the interplay between the complex quartz surface and the atoms presents a challenge for both theoreticians and experimental chemists, leading to ongoing discussions and research using homologs to better understand its behavior [42]. Astatine, classified as a metalloid, is an ideal candidate for studying surface reactions on SiO_2, as it exhibits both metallic and non-metallic chemical behavior.

Ideally, the quartz surface is chemically inert and consists only of siloxane rings made up of [SiO_4] tetrahedra, linked by flexible Si–O–Si bonds. However, the real fused silica surface is amorphous and contains reactive sites, such as oxygen vacancies or undercoordinated silicon atoms [49]. On non-reactive sites, the adsorption of H_2 and O_2 is unfavorable, while H_2O can adsorb on fused silica at standard

Table 1 Summary of the adsorption enthalpy values for superheavy elements (Z = 112–118) and their lighter homologs

Species	$-\Delta H_{ads}$(Au)/kJ/mol	$-\Delta H_{ads}(SiO_2)$/kJ/mol	References	Comment
Hg	98 ± 3	43 ± 1	[31, 32]	–
Cn	52^{+4}_{-3}	–	[38]	–
Tl	270 ± 10	158 ± 3	[33, 39]	–
Nh	–	58^{+8}_{-3}	[27]	–
Pb	–	222 ± 8, 207 ± 21	[40, 41]	–
Fl	–	–	[42, 43]	Deposited on Au
Bi	269 ± 7	109	[35, 40]	–
Mc	–	54^{+11}_{-5}	[27]	–
Po	250 ± 7	85^{+3}_{-2}	[35, 36]	–
Lv	–	–	–	–
At	154 ± 5	123 ± 10	[37]	–
Ts	–	–	–	–
Rn	27 ± 3	21 ± 4	[31, 44]	Adsorption on ice
Og	–	–	–	–

conditions and even dissociatively react with Si–O–Si bonds, leading to the formation of silanol groups (Si–OH). Treatments with H_2 also increases the degree of surface hydroxylation [50]. Depending on the surface hydroxylation degree, multiple configurations for silanols are possible: *Isolated* silanols are single, terminal silanol groups. *Vicinal* silanol groups are neighboring SiOH groups (HO–Si–O–Si–OH). Two silanols that are in close range may form H-bonds, leading to the *H-bonded* or *bridged* configuration. Lastly, *geminal* silanols are two hydroxyl groups on one Si-atom [=Si-$(OH)_2$]. The concentration of silanols of each configuration varies with the thermal treatment and temperature. Temperatures higher than ~ 1200 °C result in the complete removal of silanol groups [51, 52]. O_2 does not influence the fused silica surface, but can contain H_2O impurities, which can cause adsorption of surface water or hydroxylation, as described above.

Past gas–solid chromatography experiments on Au, quartz and Se surfaces [37, 53] using inert or reactive gases have shown strong interactions of At species with Au surfaces, consistent with theoretical predictions [46, 53]. Several deposition zones were observed in single-atom thermochromatography studies of At on quartz surfaces [37]. However, in gas-chromatography setups, no information on the speciation can be obtained and thus it is not possible to differentiate between two species with similar adsorption properties. The deposition zones were tentatively assigned to originate from the deposition of different At species, such as elemental At, AtOH and AtO_2 [37, 53].

In this study, we explore the volatility of At, its reactivity in the gas phase and the interaction with different fused silica surfaces. The present study focuses on the influence of surface chemical reactions on the adsorption properties and chemical forms of deposited At species. This research contributes to past and future experiments with superheavy elements and their homologs, as we study the processes occurring on the surface, which were neglected in previous experiments. To cope with the inherent absence of direct information on the speciation, we carefully choose different experimental conditions that allow us to formulate a well-founded hypothesis on the chemical state of the At species in question.

Experimental

All experiments in this work were carried out at the U-120M cyclotron facility at the Nuclear Physics Institute of the Czech Academy of Sciences in Řež, Czech Republic (UJF). ^{3}He beams with an energy of 45–50 MeV and a current of 300–500 µA irradiated thin Bi_2O_3 targets (areal density of Bi ≈ 420 µg/cm^2), produced by the thermal deposition on 5 µm-thick Ti backings. Astatine radioisotopes were produced in the nuclear fusion-evaporation reactions ^{209}Bi(^{3}He, 4-5 n)^{207,208}At with cross-sections of ~ 1 b for ^{207}At and ~ 500 mb for ^{208}At [54]. The beam entered and penetrated the Ti-backing foil and then entered the Bi_2O_3 target layer. The reaction products recoiling from the target were thermalized within the gas volume of the recoil chamber (RC), utilizing He as the stopping and as carrier gas, or implanted in a Ti catcher foil (thickness = 2.5 µm) placed directly behind the target.

In case of on-line experiments, following the Recoil Chamber, the At atoms were flushed to the experimental setup through a 10 m long, polytetrafluoroethylene (PTFE) capillary (inner diameter, i.d. = 2 mm), using typical He flow rates of 30–50 mL/min. Pure He (Linde, 99.9999%), purified by purification cartridges (Spectromol Oxysorb® and Hydrosorb®), to reduce H_2O and O_2 content was used. Two mass flow controllers (1179 MKS) regulated the inlet of He into the recoil chamber and also the inlet of reactive gases into the experimental setup. The following reactive gases were added in front of the chromatographic column: O_2 (99.995%), He (99.996%)/H_2(99.999%) 60:40. The gas flow rate and pressure were monitored after the column. Figure 1 shows a schematic of the various setups used in this study.

An overview of all experimental parameters and the type of setup (A–D, see, Fig. 1) is given in Table 2.

In this study, we utilized five forms of quartz, summarized in Table 3: quartz annealed in air at 1000 °C for 24 h 1.5 years prior to the experiment (Q_{Air}); quartz annealed in air at 1000 °C for 24 h 1 month prior to the experiment (Q_{Air2}); untreated quartz stored in air (Q_{UT}); quartz annealed in humid He flow at 1000 °C (Q_{H2O}) and quartz produced through the electromelting of quartz granulate (Q_{EM}). The surface hydroxylation varies between the quartz types [51, 55]. Q_{Air} and Q_{Air2} are likely dehydroxylated due to the annealing at 1000 °C prior to the experiment. Q_{EM} should have the lowest concentration of hydroxyl-groups due to the electromelting process. Q_{UT} likely features an irregular and hydroxylated surface. The surface of Q_{H2O} is expected to be most hydroxylated due to the humid conditions during annealing.

For thermochromatography experiments, open quartz tubes (i.d. = 4 mm, length L = 82–90 cm) were employed. Astatine was transported through the 10-m long PTFE capillary from the recoil chamber at room temperature with pure He gas. It was then flushed through the chromatography column, which was maintained at different temperatures in different experiments to investigate the thermochromatographic behavior of the present At. In off-line experiments, the Ti catcher foil was placed inside the hottest part of the chromatography column to evaporate At at temperatures between 680 and 1030 °C. In experiments involving reactive gases, these gases were introduced into the system 4 cm before the entrance of the quartz column,

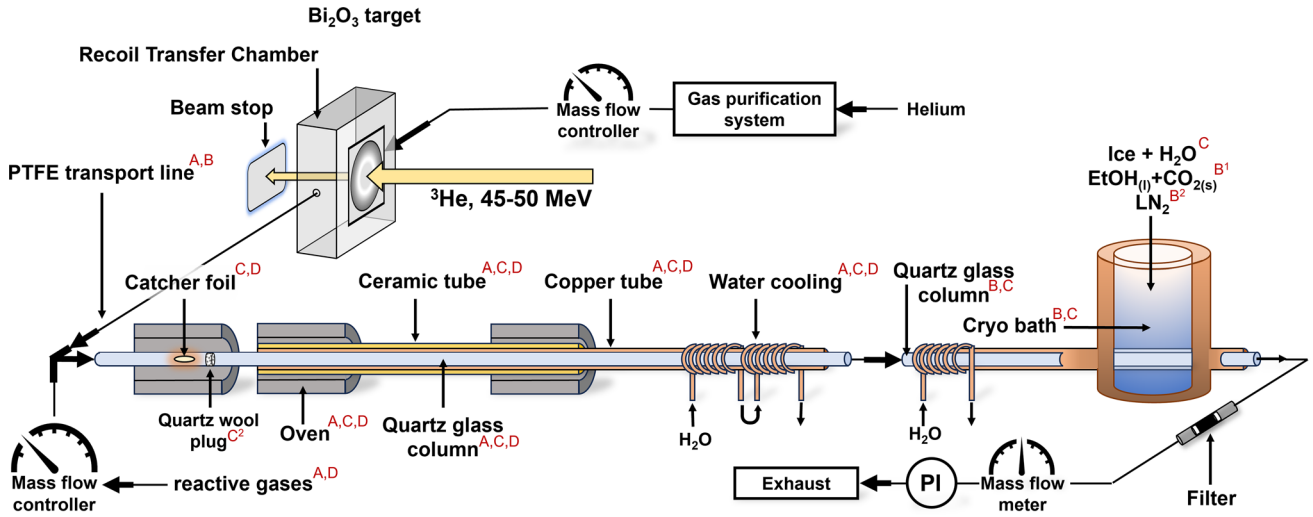

Fig. 1 Schematic of the thermochromatography setup used in this work. The parts marked with red letters were used in specific experiments (cf. Table 2). Other parts of the experimental setup were used in all experiments. He flushes through the gas purification system and into the recoil chamber, where the Bi_2O_3-target is irradiated with a ^{3}He beam. In on-line experiments, the recoil products were thermalized in the recoil chamber and transported via a 10 m PTFE capillary to the chromatography setup. Reactive gases were admixed to He before the chromatography column. The column is heated by three ovens. In off-line experiments the first oven serves as evaporation oven for the isotopes in the catcher foil. A copper and a ceramic tube, as well as water cooling help to establish a smooth temperature gradient along the column. Optionally, a cooled column was installed after the hot column (range T = 17–173 °C). A charcoal filter trapped At species not adsorbed in the column(s). The mass flow rates were controlled by mass flow controllers. The gas flow rates and pressure were monitored at the exit of the experimental setup by a mass flow meter and a pressure indicator (PI). (Color figure online)

Table 2 Overview of all experiments, including experimental conditions and setup as pictured in Fig. 1

#	Chromatogram displayed in	Setup (Fig. 1)	He/sccm/min	Reactive gas	Quartz	Time/min	Method
1	Figure 2a	A	50	–	Q_{Air}	91	On-line
2	Figure 2b	A	45	H_2: 5 mL	Q_{Air}	122	On-line
3	Figure 3a	A	45	O_2: 5 mL	Q_{Air}	141	On-line
4	Figure 3b	B	45	H_2O	Q_{EM}	104	On-line
5	Figure 4a	B^1	30	–	Q_{UT}	117	On-line
6	Figure 4b	B^2	50	–	Q_{UT}	131	On-line
7	Figure 5a	C	50	–	Q_{EM}	60	Off-line
8	Figure 5b	C^1	50	–	Q_{EM}	122	Off-line
9	Figure 6	D	50	–	Q_{H2O}	89	Off-line
10	–	A*	500	–	Q_{Air2}	180	On-line

Small numbers indicate only a minor change in the setup, e.g. a different cooling solution or insertion of the quartz wool plug

*Similar to setup A, but with positive gradient (T = 20–515 °C)

regulated to 10% of the total gas flow rate via a valve. H_2O vapor was added to the carrier gas by flushing He gas through a T-part connected to a cylinder heated to 50–60 °C filled with H_2O. The whole transport line and the setup were designed such that fused silica was the first surface, which At encountered after passing the PTFE capillary. In experiments #4-8 (Table 2), a second cooled quartz column (L = 50 cm) was added, connected to the primary column by a PTFE capillary (L = 40 cm, i.d. = 4 mm). The At, which was not adsorbed in the chromatographic column was trapped in a charcoal filter.

A defined temperature gradient was established along the chromatographic column by a set of tubular furnaces. Copper tubes around the silica chromatography columns were used to establish a smooth temperature profile along both columns. For the hot part of the column, the copper tube was inserted in a ceramic tube, fitting the diameter of the tubular furnaces. In the thermochromatography experiments, the

cold end of the copper tube was cooled by water (cf. Fig. 1). In experiments where the temperature gradient extended to temperatures below room temperature, the columns were fit inside a copper tube, which was held at room temperature by water at the entrance. The end of the column was placed in a bath filled either with ethanol/dry ice or with liquid nitrogen.

In one experiment (#8), a quartz wool plug was placed in the quartz column in the hottest area to enlarge the quartz surface, acting as a reaction zone. To determine if any aerosol particles are present, which would lead to non-chromatographic transport of any attached radionuclide through the column, the charcoal filter was replaced by a tube lined inside with Au foil. Astatine, not attached to aerosols, would deposit on the Au surface, while aerosol particles with At would pass the surface without deposition. In two experiments (#10), At was fed through the column, along which a positive temperature gradient from 20 to 515 °C was established (not depicted in Fig. 1).

The chromatography column was pre-heated to establish the temperature gradient and flushed with the desired carrier gas prior to the experiments, which then lasted for 1–2 h. In on-line experiments, the At isotopes produced by irradiation were continuously transported to the column. In off-line experiments, the catcher foil was first transferred to the setup and then heated to release At at the beginning of the column with the gas-flow for the duration of the experiment. At the end of the chromatography experiment, the gas flow was stopped, and the column was cooled down by removing the column from the ovens through the cold end. To prevent desorption of volatile At species adsorbed in the cooled column, all columns were frozen by liquid nitrogen before segmentation. Subsequently, the tube was cut into pieces and sealed in either plastic tubes or bags. Depending on the specific activity and the position of the deposition peaks, which were roughly identified with a Geiger-Müller-counter before cutting the column, a different segment length was selected: (2.0 ± 0.2) cm, (4.0 ± 0.2) cm or (8.0 ± 0.2) cm. Gamma spectra of each segment and of the charcoal filter were obtained using a germanium detector GMX20P4-70 from ORTEC. A 3D-printed sample holder ensured that segments of various length and the filter were measured in the same detector geometry. Each sample was measured for 1–5 min. Representative gamma spectra can be found in the supplementary materials.

To obtain chromatograms, the net areas of peaks in the gamma spectra at 178, 236, 301, 588, 660, 686, 814, 992 keV (if present) from the isotopes ^{207,208}At were integrated. The specific activities per column length unit, obtained for each individual column segment were corrected for radioactive decay and normalized to the total deposited and measured activity by the live time of the measurement. By comparing the experimental distributions with the results of Monte Carlo simulations [56, 57], using experimental parameters as input values and adjusting the adsorption enthalpy for the best agreement, the adsorption enthalpy values of the deposited species were determined. The Monte Carlo simulations took the continuous production of astatine in on-line experiments into account. The simulations were also adapted to include a single-step process, representing a change in interaction strength with the quartz surface [57]. Invoking such a mechanism was necessary to reproduce the absence of deposition in the cold zone at the beginning of the columns. Since this model only accounts for a single reaction of species A to species B, the deposition peaks of experiments with more than two deposition peaks and the additional activity in the filter were simulated using the standard mobile adsorption model [56]. For some simulated deposition peaks, the activity was normalized to fit the distinct peak in the experiment, since in some experiments, multiple peaks were observed. The sum of the simulated relative activity can therefore be lower than 100%, which does not interfere with the further evaluation. The error margin was defined as the range of enthalpies for which the simulated deposition peak overlapped with at least 50% of the experimentally observed peak. This approach reflects a physically meaningful uncertainty based on peak position and thus deposition temperature, rather than a purely statistical 1σ standard deviation.

Results and discussion

The results of the experiments are presented as thermochromatograms, in which the temperature gradient, the measured deposition and the simulated deposition along the column are overlaid. Figure 2 shows the deposition of At on a quartz column, which had been annealed at 1000 °C in air 1.5 years prior to the experiments (Q_{Air}).

Furthermore, experiments with oxidizing carrier gases were performed. The results of measurements in He/O_2 atmosphere and moist He are shown in Fig. 3.

In experiments #1–3, the gap between the two ovens at the beginning of the column resulted in a v-shaped temperature profile. The drop in temperature did not interfere with the evaluation, as no activity was detected in this area. In further experiments, better insulation was achieved, and the temperature gradient was smoothed. In the experiment conducted in He (Fig. 2a), 60% of the At activity reached the charcoal filter, while the remaining 40% deposited in the last 2 cm-segment of the quartz column. Under a H_2-containing atmosphere (Fig. 2b), approximately 50% of the At passed through the entire column, with only minor deposition observed at room temperature and around 28% of activity detected in the final 2 cm of the column. Since the temperature profile is flat over the last 14 cm and room temperature is thus established well

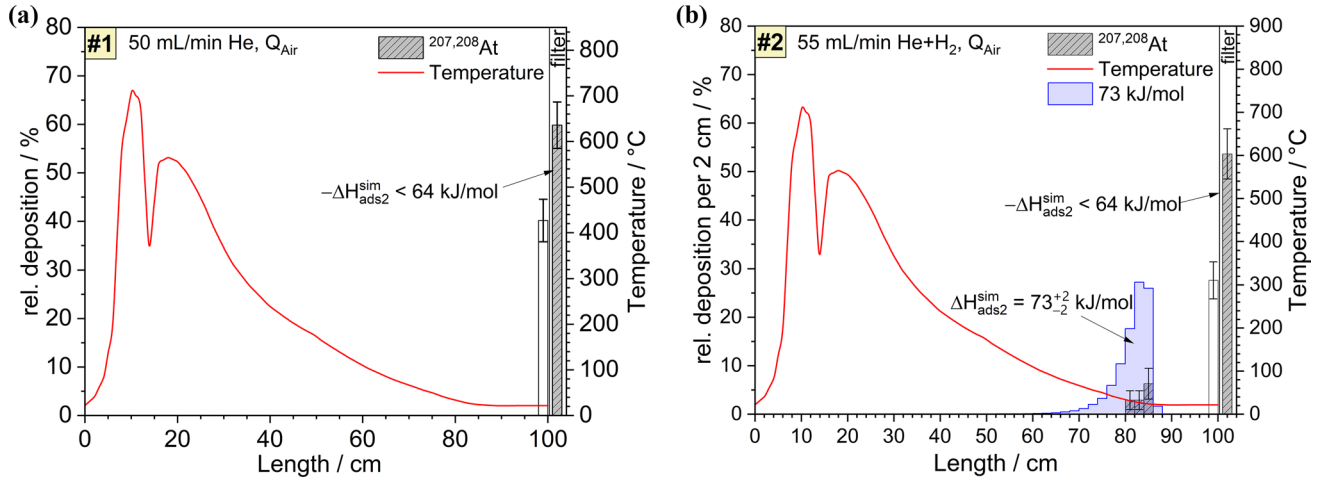

Fig. 2 Experiment #1 (panel a) and #2 (panel b): Thermochromatograms of ^{207,208}At in **a** He and **b** He/H_2 atmospheres on quartz glass Q_{Air}. The experimental deposition is shown in grey, the simulated deposition using the Monte Carlo method with $-\Delta H^{sim}_{ads2}(At) = 73$ kJ/mol is shown in blue and the temperature is shown in red. Monte Carlo simulations with $-\Delta H^{sim}_{ads2}(At) < 64$ kJ/mol lead to 100% deposition in the filter. White deposition peaks were excluded from evaluation (discussed below). (Color figure online)

before the last segment, this deposition is likely due to some gas flow turbulence in front of the charcoal filter. In contrast, the experiment with O_2 (Fig. 3a) resulted in only 20% of the At reaching the charcoal filter, with the majority (about 80%) depositing in the last 12 cm of the column, at temperatures ranging from 40 to 20 °C. It cannot be excluded that the last segment suffered from the same increased deposition due to the same turbulences as observed in #1 and #2. In moist He atmosphere (Fig. 3b), At deposited at temperatures below 50 °C, with a minor fraction being deposited at the beginning of the ice-cooled column (17–3 °C, cm 100–124). No At passed to the charcoal filter. Condensation of water was observed in the region of the deposition, leading to the conclusion that At might not have been deposited, but rather dissolved in H_2O on the surface. Two additional control experiments, where a positive temperature gradient from 20 to 515 °C was established, were performed to confirm the previously observed high volatility of At. 100% of the At activity passed through the column into the filter without any detectable deposition on the quartz surface (Exp. #10, setup **A***). In the experiment using a 10 cm-long Au column, ~ 96% of the total measured activity deposited in

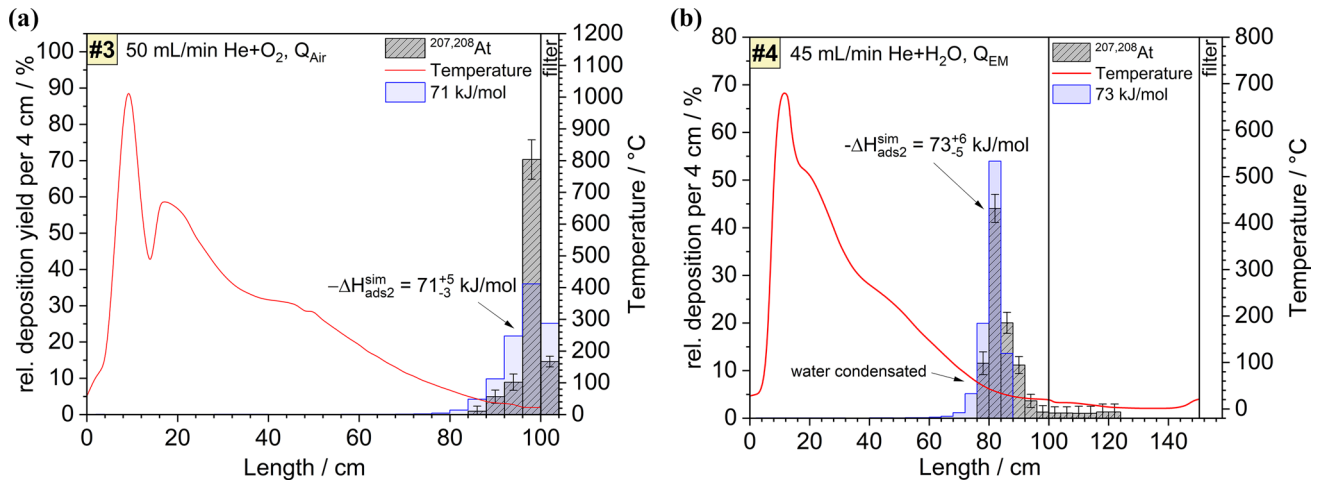

Fig. 3 Experiment #3 (panel a) and #4 (panel b): Thermochromatogram of ^{207,208}At in O_2 atmosphere on quartz glass annealed at 1000 °C (**a**) and in moist He on electromelted quartz glass Q_{EM} (**b**). The experimental deposition is shown in grey, the simulated deposition using the advanced Monte Carlo method including chemical reaction with the surface is shown in blue and the temperature is shown in red. (Color figure online)

the Au surface, which contradicts the presence of aerosol transport.

The absence of At deposition above 50 °C in all experiments #1–4 indicates that At does not form any non-volatile species in the gas phase, even in the presence of reducing gases (H_2) or oxidizing gases (O_2, H_2O) at elevated temperatures up to 1000 °C. In all experiments on surface Q_{Air} (Fig. 2), the At was found in the last segment of the column. However, in H_2O-containing atmosphere, approximately 80% of the At deposited before reaching the last 4 cm-long segment, with significant deposition occurring between 88 and 96 cm. If At entered the column in the same state in which it ultimately deposited, one would expect deposition at the very beginning of the column at room temperature, before reaching the first oven set. However, no substantial deposition was observed in the cold zone at the start of the column during any of the on-line experiments. This strongly suggests that the deposited species is different from the species entering the column.

Using advanced Monte Carlo simulations [57] and considering the continuous production and injection of At in on-line experiments, the adsorption enthalpy of the At species in the column was determined to be $-\Delta H_{ads} = 71^{+5}_{-3}$ kJ/mol and 73^{+6}_{-5} kJ/mol for experiments with O_2-containing atmosphere and moist He (#3 and #4, Fig. 3). Note, that the Monte Carlo simulation does not account for the condensated water that formed during experiment #4 and was performed assuming dry conditions and a clean surface. The value for the adsorption enthalpy (which would be an upper limit in case of dissolution of the astatine species in water) is thus excluded from further evaluation.

The volatile species, which passed through the column and was retained by the charcoal filter, was studied in low temperature experiments on quartz Q_{UT} (#5 and #6, Fig. 4). Using pure He as carrier gas and a cooling solution of dry-ice/ethanol (with the lowest temperature in the column being − 57 °C) resulted in deposition of the At species at (15 ± 6) °C, while 30% of At still passed the column and was detected in the filter (Fig. 4a). While in #5 (Fig. 4a) ~ 30% of the activity still passed through the column cooled down to − 57 °C, even the most volatile species ultimately deposited when the column was cooled down to − 173 °C in #6 (Fig. 4b). Deposition was observed in a wide temperature range between − 40 and − 135 °C. No At was detected in the charcoal filter, indicating complete deposition of the most volatile species within the column (Fig. 4b).

During experiment #5, a leak occurred in the Recoil Chamber, possibly leading to H_2O and O_2 contamination of the gas phase. The deposition of the species at 15 °C is best fit by Monte Carlo simulations with an adsorption enthalpy of $-\Delta H_{ads} = 68^{+4}_{-2}$ kJ/mol, and is thus assigned to the same species observed in the experiments with O_2 (cf. Fig. 3a), $-\Delta H_{ads}=73^{+6}_{-5}$ kJ/mol and H_2O, $-\Delta H_{ads} = 71^{+5}_{-3}$ kJ/mol (Fig. 3b). In experiment #5 (Fig. 4a), the most volatile species passed over surfaces held at temperatures down to − 57 °C without deposition, yielding an upper limit of $-\Delta H_{ads}$ of 43^{+2}_{-2} kJ/mol, derived from the Monte Carlo simulation based on the relative At yield of 30% found in the filter. However, the results shown in Fig. 4b (#6) indicate a more complex behavior. Here, over 50% of the activity was deposited at a temperature of approximately $T_{dep} = -60 \pm 9$ °C, leading to an estimated adsorption enthalpy $-\Delta H_{ads} = 54^{+4}_{-4}$ kJ/mol. This is notably higher than the values suggested by the results of Fig. 4a, where no

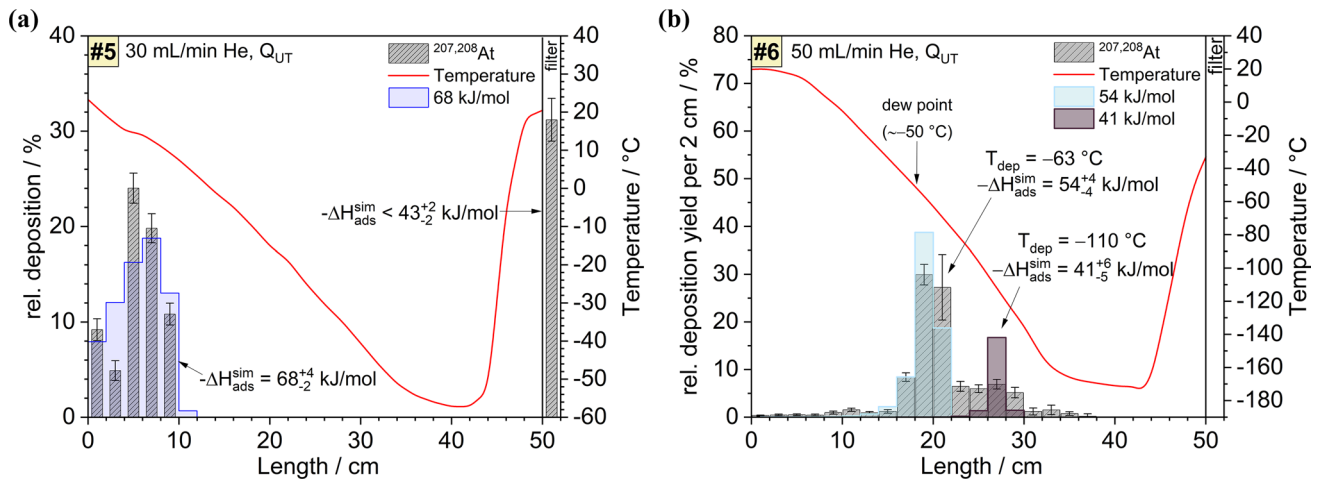

Fig. 4 Experiment #5 (panel a) and #6 (panel b): Thermochromatograms of ^{207,208}At in He on quartz glass (Q_{UT}) and gradient reaching from ambient temperature to − 57 °C (**a**) and − 173 °C (**b**). The experimental deposition is shown as grey bars, the simulated deposition using the Monte Carlo method is shown by the stepped lines and the temperature profile is shown as red line. (Color figure online)

deposition occurred at − 57 °C. The discrepancy between these two experiments indicated that additional factors may have influenced the deposition process. We hypothesize that the divergence in the deposition behavior starting at − 40 °C is explicable by the assumption of the formation of ice on the SiO_2 surface. According to the estimated dew point of − 50 °C (based on previous experiments using similar gases and cleaning cartridges) and experimental conditions, we suspect that a small amount of water vapor present in the system deposited at this temperature, forming a thin ice layer. The ice formation alters the surface properties, and provides additional deposition sites for At, leading to the increased deposition observed at − 60 ± 9 °C. Additionally, the continuous ice formation during the experiment can cause incorporation of deposited At into the ice layer.

At even lower temperatures, Fig. 4b shows another deposition peak. Assuming that the main amount of water was deposited between − 60 and − 90 °C, partially incorporating At during the formation of ice, the water concentration at lower temperatures is much smaller, leading only to a very thin layer of ice.At − 100 to − 130 °C, At is reversibly adsorbed on the ice-covered surface and not incorporated into the ice. Given that no hot surfaces or reactive gases were employed in these experiments, and the species passed through a cold zone prior to any reaction (Figs. 2 and 3), we assign the most volatile species to elemental At(0). Based on simulations of the low-temperature part of the deposition peak, the adsorption enthalpy of At on ice is estimated to be $-\Delta H^{ice}_{ads.}(\mathrm{At}) = 41^{+6}_{-5}$ kJ/mol, while its adsorption enthalpy on bare SiO_2 remains lower than $-\Delta H^{SiO_2}_{ads.}(\mathrm{At}) < 43$ kJ/mol, as indicated by the lack of deposition at − 57 °C in #5, Fig. 4a. Our findings align with theoretical calculations, which propose that elemental At is the most volatile species with smaller interaction strength on both vicinal and geminal quartz with predicted $-\Delta H^{SiO_2}_{ads.}(\mathrm{At}) = 20$ kJ/mol and 26 kJ/mol, respectively [58], but also with experimental findings from the production and separation of At [5, 59, 60].

The less volatile non-elemental species, deposited at around room temperature, has an adsorption enthalpy of 71 ± 5 kJ/mol, based on the average of two experiments (Figs. 3a and 4a). The minor deposition in Fig. 2b at around 80–85 cm and the measurement with condensed water (Fig. 3b) were not taken into account, but yield identical adsorption enthalpies within error bars. In our experimental setup, no information on the speciation can be obtained and thus it is not possible to differentiate between AtH, At(I)OH, At(III)OOH or At(V)O_2OH. According to [58], At(III)OOH, At(V)O_2OH as well as further oxides are expected to exhibit significantly stronger adsorption and should adsorb well above room temperature on vicinal quartz. Since a minor deposition of the species was observed in He/H_2 atmosphere at room temperature, we exclude species with oxidation states of greater than (+ I), since those species would easily be reduced in the given conditions [46] and deposit already at much higher temperatures. The formation of AtH from At + H_2O is energetically not favored and unlikely under oxidizing conditions [46]. The presence of the species was prominent in experiments with O_2 and H_2O, the oxidized species At(I)OH/HAt(I)O is assigned (further referred to as AtOH) Thus, only AtOH remains as the possible species. The presence of AtOH in experiments with H_2, O_2 and H_2O atmospheres points to the formation of AtOH through surface-mediated oxidation. We propose, that AtOH was not formed in the gas-phase but rather by At reacting with hydroxyl groups in surface-mediated oxidation. Results of theoretical calculations show, that AtOH along with AtH is predicted to be the second most volatile species after elemental At, with the adsorption enthalpy being about 20 kJ/mol larger than that of elemental At [58], which matches our findings. Other sources also report deposition of some At species around room temperature [59, 60].

These findings suggest that the interplay of surface hydroxylation and gas composition plays a key role in the formation of AtOH, which presumably formed in reactions on the quartz surface at higher temperatures in presence of reactive gases (H_2, O_2 and H_2O). The presence of H_2 or H_2O (including trace impurities) enhance surface hydroxylation at elevated temperatures. Since silanol groups act as reactive sites that promotes the adsorption and oxidation of elemental At, their presence facilitates the formation of AtOH. In both experiments, depositions of AtOH were observed, while elemental At was trapped in the charcoal filter. However, the fraction of AtOH was significantly lower in H_2-containing atmosphere compared to the O_2-containing atmosphere. This behavior is consistent with the fact that hydroxylation of quartz using H_2 is thermally activated and kinetically slow. Given the short experimental timescale, surface hydroxylation is limited under H_2, resulting in only minor deposition of AtOH in experiment #2. In contrast, even small amounts of water impurities from the Recoil Chamber can rapidly hydroxylate the surface, causing the more efficient formation of AtOH in #3, Fig. 3a. Based on these observations we report the adsorption enthalpy as $-\Delta H^{SiO_2}_{ads.}(\mathrm{AtOH}) = 71 \pm 5$ kJ/mol.

In off-line experiments, further chromatograms were acquired to study the formation of At (hydr)oxides (Fig. 4) and compare the reactivity of different quartz surfaces, namely electromelted quartz and quartz previously treated with water vapors, cf. Table 1. Additionally, in experiment #8, a quartz wool plug was introduced into the column just behind the catcher foil to increase the retention time and thus the time available for a potential chemical interaction between At species and the quartz surface. For these

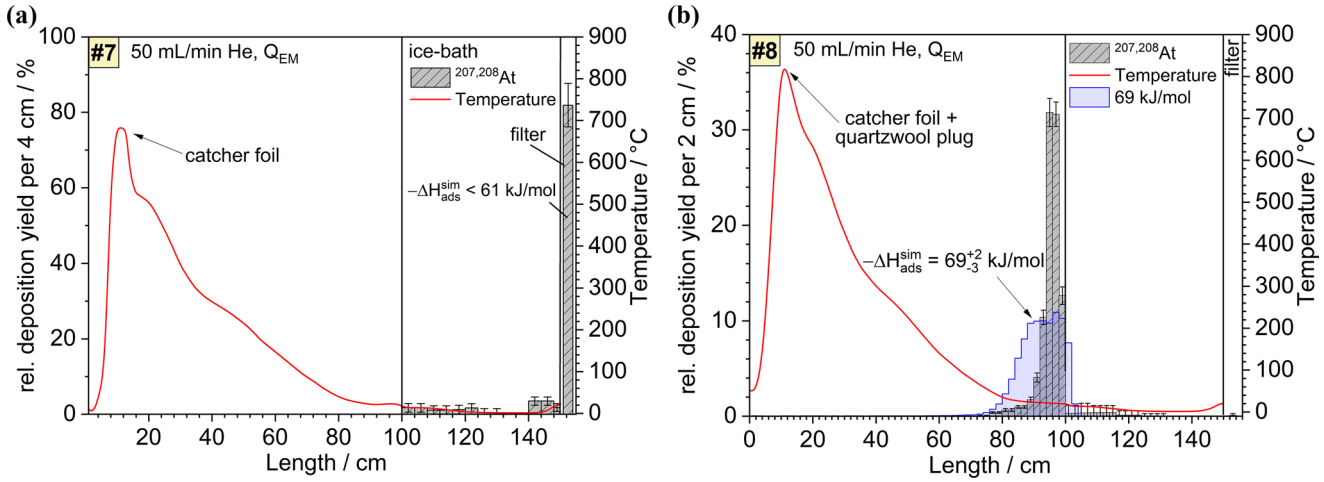

Fig. 5 Experiment #7 (panel a) and #8 (panel b): Thermochromatograms of ^{207,208}At in He on electromelted quartz glass Q_{EM} without quartz wool plug (**a**) and with quartz wool plug inserted behind the catcher foil (**b**). The experimental deposition is shown in grey, the simulated deposition using the Monte Carlo method is shown in blue and the temperature is shown in red. (Color figure online)

off-line experiments (#7–9, Table 2), Ti catcher foils were placed inside a column at a position of 12–14 cm, where the temperature maximum occurred. This position was also set as the starting point for atoms in the Monte Carlo simulation.

On Q_{EM} (electromelted quartz, #7, cf. Fig. 5a), no deposition was observed in the column from 700 to 20 °C. In the adjacent section, cooled by an ice-bath down to about 0 °C, 20% of the activity was deposited as AtOH, while 80% passed to the filter. Figure 5a indicates that the At captured in experiment #1–2 (Q_{Air}, He, Fig. 2a) at the end of the column is indeed a contamination. As no differences are observed when comparing experiment #7 to #1, we conclude that the species evaporated from the Ti catcher foil is identical to the species transported from the Recoil Chamber.

In experiment #8 (cf. Fig. 5b), a hot quartz wool plug was inserted into a Q_{EM} column, acting as a reaction zone with increased surface. In Fig. 5b, a large deposition peak at room temperature is visible, while no significant At deposition occurred in the 50 cm long cooled column, in the quartz wool plug or in the charcoal filter, as all At was oxidized to AtOH. The quartz wool plug, held at 800 °C, offers chemically reactive sites, on which AtOH is formed. In contrast, the electromelted quartz surface of the column is not reactive (Fig. 5a) so that only At compounds formed in the hot reaction zone deposited. The reaction products formed in the hot quartz wool plug desorb from its surface and deposit fully at temperatures slightly above room temperature in the column. Thus, the observed deposition corresponding to the adsorption enthalpy of 69^{+2}_{-3} kJ/mol is once more assigned to AtOH, formed in the reaction with quartz wool plug at 800 °C and transported to this deposition zone.

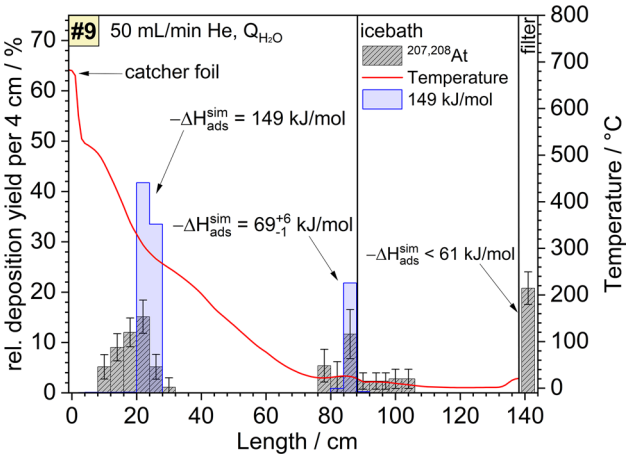

Fig. 6 Experiment #9: Thermochromatogram of ^{207,208}At in He on quartz previously treated with H_2O (Q_{H2O}). The experimental deposition is shown in grey, the simulated deposition using the advanced Monte Carlo method including chemical reaction with the surface is shown in blue and the temperature is shown in red. (Color figure online)

Table 3 Description of quartz columns used in the experiments

Name	Annealed	In gas	Comments
Q_{Air}	1000 °C, 24 h	Air	Ilmasil®, annealed 1.5 years prior to the experiments
Q_{Air2}	1000 °C, 24 h	Air	Annealed 1 month prior to the experiments
Q_{UT}	Untreated	–	–
Q_{EM}	Electromelted	–	–
Q_{H2O}	1000 °C	He/H_2O	Treated with H_2O for 20 h

Annealing the quartz surface in moist He gas and thus increasing the concentration of reactive hydroxyl groups on the surface led to the highest deposition temperature of At, not only in this series of experiments (#1–#10), but in all yet reported thermochromatography studies (Fig. 6).

On this activated surface, 48% of At deposited at temperatures between 300 and 500 °C, as well as at room temperature (32%), with ~ 20% passing into the filter. This high-temperature deposition in Fig. 6 can be explained by either of the following two possible mechanisms:

1. Deposition of an At species: On the surface At likely reacts with silanol groups (Si–OH), forming oxidized species such as $AtO_x(OH)$ (x = 0–2). The resulting reaction products might be non-volatile at temperatures of 300–500 °C, preventing further transport in the column. However, the theoretically predicted adsorption enthalpy values of At oxo-hydrides ($-\Delta H^{theo.}_{ads.}$(AtO(OH)) = 99 kJ/mol [58]) suggest that oxidized At species should desorb and be available for further transport at these temperatures. Furthermore, comparing the adsorption enthalpy of the species responsible for this high-temperature deposition with theoretical and experimental studies indicates that At species typically exhibit weaker interactions with the surface. Thus, we consider adsorption alone to be insufficient to fully explain this phenomenon.
2. Chemical bonding to the surface: After reacting with the surface's functional groups, At is chemically bound via At–O–Si or At–Si bonds. At temperatures between 300 and 500 °C all types of silanols (isolated, vicinal, H-bridged, geminal) coexist. This leaves a variety of possible reaction sites for At. The formed bonds are apparently sufficiently strong that they are not broken at temperatures below 400 °C. This implies that At is not simply adsorbed but is chemically bound to the surface. The formation of such chemical bonding likely involves overcoming an activation energy barrier. Additionally, the desorption enthalpy may differ from the adsorption enthalpy due to variations in surface composition and specific adsorption positions of the atom. This could account for the broad deposition range observed between 500 and 300 °C.

This high-temperature deposition is strongly pronounced on Q_{H2O}, while it is completely absent on the electromelted quartz Q_{EM}, even when a quartz wool plug is added to the column. This indicates a dependence of the formation of the high-temperature deposition zone and the concentration of hydroxyl groups on the surface. Two key observations support this conclusion:

1. The deposition occurs only on hydroxylated surfaces (Q_{H2O}), not on the dehydroxylated Q_{EM}.
2. A previous study (which does not give specific information on the used quartz surface) reports no deposition in this temperature range [37], rendering simple adsorption of oxidized species unlikely.

Likewise, theoretical predictions of values of the adsorption enthalpy for oxidized species are not consistent with the deposition in this temperature range [58]. Instead, our results suggest that the high-temperature deposition is best explained by chemical bonding of At to the surface via At–O–Si or At–Si, rather than adsorption of any oxidized At species. Thus, for desorption to occur, a chemical bond must be broken, requiring significantly more energy than that needed to desorb At oxo-hydrides.

In the experiment #8 (Fig. 5b) with the quartz wool plug in the high temperature zone (800 °C) only one deposition zone with $-\Delta H^{SiO_2}_{ads.} = 69^{+2}_{-3}$ kJ/mol was observed. In the reaction of At with the reactive quartz surface, two outcomes are possible: a chemical bonding of At to quartz and possibly the desorption by bond breaking leading to AtOH or At. Obviously, AtOH was quantitatively formed in the reaction between hydroxylated quartz and At on the large, reactive surface of the quartz wool plug. This deposition aligns with the deposition of At species in experiments with reactive gases ($He + O_2$, $He + H_2$ and $He + H_2O$) and is assigned to AtOH. However, in experiment #8, the temperature was high enough (800 °C) to desorb AtOH by the breaking of the chemical bond between this At species and the quartz surface, in contrast to the situation in experiment #9, where the high temperature deposition was observed (cf. Fig. 6). This supports our hypothesis that chemical reactions of At with surface hydroxyl groups occurred. In this specific case, approximately 80% of all At reacted chemically with these groups, forming an oxidized species that is less volatile than elemental At, and which deposited around room temperature, rather than passing the column.

As the height of the energy barrier for the reaction of species A to species B is unknown [61, 62], a nominal value of 100 kJ/mol was specified in the Monte Carlo simulation, as this led to complete conversion of species A–B in the hot zone of the column. The adsorption enthalpy of the initial species A (elemental At) was set to $-\Delta H^{sim}_{ads1} = 43$ kJ/mol, the lowest limit for the adsorption value determined in this work (see Fig. 4). These parameters produced simulated chromatograms, in which species A ($-\Delta H^{sim}_{ads1} = 43$ kJ/mol) completely passed over the cold zone at the beginning of the column, reacted in the hot zone and deposited as AtOH at lower temperatures.

The deposition observed between 500 and 300 °C in experiment #9 in Fig. 6 was absent in exp. #8, Fig. 5b, suggesting that this deposition does not result from reversible physisorption of a highly oxidized species but rather from strong chemisorption of At with the surface. This further

indicates that once an oxidized At species detaches, it does no longer undergo reactions with the surface. During the experiment #4 (Fig. 3b) with water vapor, the H_2O content in the carrier gas increased the hydroxylation of the surface at high temperatures, creating more reactive sites and thus promoting the formation of oxidized species.

The sublimation enthalpy $\Delta H^{\circ}_{subl.}$ of a species can be estimated from the adsorption enthalpy using a correlation described in Steinegger et al. [63]. However, this correlation is only valid for cases of mobile adsorption, where no chemical transformation occurs on the surface and the species desorbs in its original chemical state. Since our results indicate transformation of the species by reaction with the surface, we refrain from the direct application of this correlation.

The many parameters that were varied in the experiments, namely temperature gradient, gas mixture and surface properties, allow to clearly observe and understand the influence of those parameters on the deposition behavior of At. In low temperature experiments, surface reactions are kinetically hindered, rendering them unlikely. Instead, elemental At is deposited on quartz, water or ice. Our findings and the assignment of the species, and the chemisorption respectively agree well with theoretical calculations. While the nature of the quartz surface is inhomogeneous, amorphous and difficult to model, the theoretical calculations still help to estimate a trend in volatility and reactivity. Calculations in [58] use a modeled quartz slab in the vicinal and geminal configuration. In reality, at temperatures between 500 and 300 °C, the state of the surface cannot be broken down to one configuration; rather it is a mixture of isolated, geminal and H-bonded silanol groups [51, 52]. Our interpretation and the general trend of volatility still confirm the calculations. The finding of AtOH deposited around room temperature confirms the results of [59, 60], where a deposition of an At species at 42 °C without gas-flow is reported in a nitrogen filled tube. Serov et al. [37] conclude that elemental At deposits at approximately 270 °C, assigning an adsorption enthalpy of $-\Delta H^{SiO_2}_{ads.}(\mathrm{At}) = 123$ kJ/mol. Furthermore, deposition peaks at $T_{\mathrm{dep}}\,(\mathrm{AtO_2}) = 63$–$73$ °C ($-\Delta H^{SiO_2}_{ads.}(\mathrm{AtO_2}) = 80$ kJ/mol) and $T_{\mathrm{dep}}\,(\mathrm{AtOH}) = -79$ °C ($-\Delta H^{SiO_2}_{ads.}(\mathrm{AtOH}) = 47 \pm 5$ kJ/mol) were assigned to oxidized species. Throughout our experimental work, we aimed to reproduce the deposition peak at 270 °C and understand the assignment of the species, but we were unable to observe a comparable deposition of elemental At or in fact any At-containing species under our conditions. The deposition at highest temperatures (300–500 °C) observed in this work is chemisorbed At, most likely bound to the surface via At-O-Si or At-Si bonds. Taking surface hydroxylation and chemisorption into account, we argue that the 123 kJ/mol species observed by Serov et al. is not elemental At but rather chemisorbed At. Our experiments in pure conditions and without any hot and reactive surfaces yield the most volatile species, which we assigned to elemental At. Our measured deposition temperature and the determined limit of $-\Delta H^{SiO_2}_{ads.}(\mathrm{At}) < 43^{+2}_{-2}$ kJ/mol agree well with the observation of Serov et al. While we report similar values, we must conclude that this deposition is elemental At, not AtOH. In our experiments, AtOH adsorbed at around room temperature and was formed by surface reaction and with traces of H_2O in the harsh conditions inside the Recoil Chamber. The adsorption enthalpy of $-\Delta H^{SiO_2}_{ads.}(\mathrm{AtOH}) = 71^{+8}_{-5}$ kJ/mol falls into the range of the reported $-\Delta H^{SiO_2}_{ads.}(\mathrm{AtO_2}) = 80$ kJ/mol. Both deposition peaks could be caused by the same species (AtOH). Similarly, Chiera et al. reported the most volatile species to be AtOH [53], purely based on the speciation of Serov et al., which we showed here to be incorrect.

In summary, the variety of the experimental conditions in this work and in the literature and the consideration of surface reactions lead us to different conclusions, compared to the works of Serov et al. and Chiera et al.: elemental At is the most volatile species, followed by the oxidized AtOH and lastly At chemically bound to the silanol groups of the surface.

Summary of experimental results and conclusion

In this study, we performed a systematic investigation of the gas-phase and surface chemistry of At using thermochromatography with carrier gases and quartz surfaces of different reactivity. Advanced Monte Carlo simulations including an activated chemisorption mechanism were used to determine the adsorption enthalpy and to model chemical reactions within the column. As an initial step, the reactivity of At in the gas-phase was analyzed using pure He as a rare gas as well as He doped with H_2, O_2 and H_2O that were added as reactive gases. The deposition of At in He and He/H_2 at room temperature differs in peak height from that in oxidizing atmospheres, indicating a reaction of At with the present traces of H_2O in O_2. Furthermore, the most volatile species was adsorbed in a dedicated low temperature experiment for which simulations yield a value of $-\Delta H^{ice}_{ads.}(\mathrm{At}) = 41^{+6}_{-5}$ kJ/mol and a limit of $-\Delta H^{SiO_2}_{ads.}(\mathrm{At}) < 43$ kJ/mol. The species was assigned to elemental At, in agreement with theoretical predictions of $-\Delta H^{SiO_2}_{ads.}(\mathrm{At}) = 26$ kJ/mol [58] and elemental At being the most volatile species. For the oxidized species AtOH, an adsorption enthalpy of $-\Delta H_{\mathrm{ads}}(\mathrm{AtOH}) = 71^{+8}_{-5}$ kJ/mol was obtained. The interaction of At with the fused silica surface was analyzed by varying the surface reactivity, using electromelted, heat-treated and H_2O-treated

surfaces, as well as inserting a quartz wool plug into the column. The results underline the importance of the consideration of surface reactions: while predominatly elemental At was observed on the less reactive electromelted quartz, At reacted with the quartz wool plug to form AtOH, which deposited in the same temperature regime as the species observed in experiments with O_2/H_2O. On hydroxylated surfaces pre-treated with H_2O vapor, At formed a chemical bond with the quartz surface. These results demonstrate that surface properties—such as those induced by annealing in H_2O vapor, producing quartz via vacuum-melting or introducing a quartz wool plug—can significantly impact the reactivity and adsorption behavior of At. This dataset also acts as a basis for comparison with future experiments with the superheavy element Ts. It contributes to all gas-chromatography experiments with superheavy elements and their lighter homologs with a better description of the complex processes that can occur in gas–solid-chromatography. Theoretical calculations suggest that Ts exhibits a similar reactivity towards O_2, H_2O and H_2 as At [46]. Based on our findings, we propose a chemical system employing an inert helium atmosphere to preserve Ts in its elemental state and to avoid oxidation. A chromatography setup combining quartz and gold surfaces is suggested to probe the volatility range of Ts from halogen-like to metallic species. The quartz surface should be de-hydroxylated to avoid the formation of TsOH in high temperatures. Alternatively, lower temperatures must be employed to suppress the reaction with the surface. Given that elemental At is volatile on quartz in temperatures down to − 57 °C and strongly interacts with Au surfaces a similar behavior is expected from elemental Ts, according to theoretical predications [46, 58]. Ts should pass over quartz surfaces at ambient temperature and adsorb only in cold temperature regimes or on a Au surface.

Supplementary Information The online version contains supplementary material available at https://doi.org/10.1007/s10967-025-10335-4.

Acknowledgements We thank the accelerator staff of the U120-M cyclotron at ÚFV in Husinec-Řež for a stable beam and Valeria Pershina for useful discussions and advice. Furthermore, we express our gratitude to the GSI target laboratory and the GSI radiation safety department.

Funding This project was funded by BMBF under Contract No. 05P21UMFN2 and by the Ministry of Education, Youth and Sports of the Czech Republic, Project Number LM2023060 "Facility for Antiproton and Ion Research—Participation of the Czech Republic (FAIR-CZ)".

Data availability The experimental data and simulation code will be made available by A. Yakushev upon request, provided that such a request is accompanied by a valid and justifiable reason for accessing the data.

Declarations

Conflict of interest The authors declare no competing interest.

References

1. Corson DR, MacKenzie KR, Segrè E (1940) Possible production of radioactive isotopes of element 85. Phys Rev 57:459. https://doi.org/10.1103/PhysRev.57.459
2. Vértes A, Nagy S, Klencsár Z (eds) (2003) Handbook of nuclear chemistry. Springer, Cham
3. Rösch F (2022) Nuclear- and radiochemistry volume 1: introduction. De Gruyter, Berlin
4. Rösch F (2022) Nuclear- and radiochemistry volume 2: modern applications. De Gruyter, Berlin
5. Lindegren S, Bäck T, Jensen HJ (2001) Dry-distillation of astatine-211 from irradiated bismuth targets: a time-saving procedure with high recovery yields. Appl Radiat Isot 55:157–160. https://doi.org/10.1016/s0969-8043(01)00044-6
6. Zalutsky R, Pruszynski M (2011) Astatine-211: production and availability. CRP 4:177–185. https://doi.org/10.2174/1874471011104030177
7. Balkin E, Hamlin D, Gagnon K et al (2013) Evaluation of a wet chemistry method for isolation of cyclotron produced [^{211}At] astatine. Appl Sci 3:636–655. https://doi.org/10.3390/app3030636
8. Eychenne R, Chérel M, Haddad F et al (2021) Overview of the most promising radionuclides for targeted alpha therapy: the "hopeful eight." Pharmaceutics. https://doi.org/10.3390/pharmaceutics13060906
9. Zalutsky MR, Reardon DA, Pozzi OR et al (2007) Targeted alpha-particle radiotherapy with ^{211}At-labeled monoclonal antibodies. Nucl Med Biol 34:779–785. https://doi.org/10.1016/j.nucmedbio.2007.03.007
10. Feng Y, Zalutsky MR (2021) Production, purification and availability of 211At: near term steps towards global access. Nucl Med Biol 100–101:12–23. https://doi.org/10.1016/j.nucmedbio.2021.05.007
11. Vanermen M, Ligeour M, Oliveira M-C et al (2024) Astatine-211 radiolabelling chemistry: from basics to advanced biological applications. EJNMMI Radiopharm Chem 9:69. https://doi.org/10.1186/s41181-024-00298-4
12. National Library of Medicine (2025) ClinicalTrials.gov. https://clinicaltrials.gov/search?intr=astatine. Accessed 21 Jan 2025
13. Pershina V (2019) Relativity in the electronic structure of the heaviest elements and its influence on periodicities in properties. Radiochim Acta 107:833–863. https://doi.org/10.1515/ract-2018-3098
14. Galland N, Montavon G, Le Questel J-Y et al (2018) Quantum calculations of At-mediated halogen bonds: on the influence of

relativistic effects. New J Chem 42:10510–10517. https://doi.org/10.1039/C8NJ00484F
15. Rothe S, Andreyev AN, Antalic S et al (2013) Measurement of the first ionization potential of astatine by laser ionization spectroscopy. Nat Commun 4:1835. https://doi.org/10.1038/ncomms2819
16. Vernon RE (2013) Which elements are metalloids? J Chem Educ 90:1703–1707. https://doi.org/10.1021/ed3008457
17. Leimbach D, Karls J, Guo Y et al (2020) The electron affinity of astatine. Nat Commun 11:3824. https://doi.org/10.1038/s41467-020-17599-2
18. Guérard F, Maingueneau C, Liu L et al (2021) Advances in the chemistry of astatine and implications for the development of radiopharmaceuticals. Acc Chem Res. https://doi.org/10.1021/acs.accounts.1c00327
19. Meyer G-J (2018) Astatine. J Labelled Comp Radiopharm 61:154–164. https://doi.org/10.1002/jlcr.3573
20. Berei K, Vasros L (1983) Organic chemistry of astatine. In: Patai S, Rappoport Z (eds) The chemistry of halides, pseudo-halides, and azides: part 1. Wiley, New York, pp 405–440
21. Otozai K, Takashi N (1982) Estimation of the chemical form and the boiling point of elementary astatine by radiogaschromatography. Radiochim Acta 31:201–204. https://doi.org/10.1524/ract.1982.31.34.201
22. Teze D, Sergentu D-C, Kalichuk V et al (2017) Targeted radionuclide therapy with astatine-211: oxidative dehalogenation of astatobenzoate conjugates. Sci Rep. https://doi.org/10.1038/s41598-017-02614-2
23. Visser GWM (1989) Inorganic astatine chemistry. Radiochim Acta 47:97–104. https://doi.org/10.1524/ract.1989.47.23.97
24. Schädel M (2006) Chemistry of superheavy elements. Angew Chem Int Ed Engl 45:368–401. https://doi.org/10.1002/anie.200461072
25. Schädel M (ed) (2014) The chemistry of superheavy elements, 2nd edn. Springer, Heidelberg
26. Türler A, Pershina V (2013) Advances in the production and chemistry of the heaviest elements. Chem Rev 113:1237–1312. https://doi.org/10.1021/cr3002438
27. Yakushev A, Khuyagbaatar J, Düllmann CE et al (2024) Manifestation of relativistic effects in the chemical properties of nihonium and moscovium revealed by gas chromatography studies. Front Chem 12:1474820. https://doi.org/10.3389/fchem.2024.1474820
28. Oganessian YT, Sobiczewski A, Ter-Akopian GM (2017) Superheavy nuclei: from predictions to discovery. Phys Scr 92(2):23003. https://doi.org/10.1088/1402-4896/aa53c1
29. Varentsov V, Yakushev A (2019) Concept of a new universal high-density gas stopping cell setup for study of gas-phase chemistry and nuclear properties of super heavy elements (UniCell). Nucl Instrum Methods Phys Res Sect A Accel Spectrom Detect Assoc Equip 940:206–214. https://doi.org/10.1016/j.nima.2019.06.032
30. Varentsov V, Yakushev A (2021) Fair-wind gas cell for the UniCell setup. Nucl Instrum Methods Phys Res Sect A Accel Spectrom Detect Assoc Equip 1010:165487. https://doi.org/10.1016/j.nima.2021.165487
31. Soverna S, Dressler R, Düllmann CE et al (2005) Thermochromatographic studies of mercury and radon on transition metal surfaces. Radiochim Acta 93:1–8. https://doi.org/10.1524/ract.93.1.1.58298
32. Lens L, Yakushev A, Düllmann CE et al (2018) Online chemical adsorption studies of Hg, Tl, and Pb on SiO_2 and Au surfaces in preparation for chemical investigations on Cn, Nh, and Fl at TASCA. Radiochim Acta 106:949–962. https://doi.org/10.1515/ract-2017-2914
33. Serov A, Eichler R, Dressler R et al (2013) Adsorption interaction of carrier-free thallium species with gold and quartz surfaces. Radiochim Acta 101:421–426. https://doi.org/10.1524/ract.2013.2045
34. Dietzel D, Yakushev A, Düllmann CE et al (2025) Single-atom-at-a-time adsorption studies of ^{211}Bi and its precursor ^{211}Pb on SiO_2 surfaces. Radiochim Acta. https://doi.org/10.1515/ract-2024-0327
35. Maugeri EA, Neuhausen J, Eichler R et al (2016) Adsorption of volatile polonium and bismuth species on metals in various gas atmospheres: Part I - adsorption of volatile polonium and bismuth on gold. Radiochim Acta 104:757–767. https://doi.org/10.1515/ract-2016-2573
36. Hermainski K, Yakushev A, Dietzel D et al Reactivity of polonium towards quartz surfaces. PCCP
37. Serov A, Aksenov NV, Bozhikov GA et al (2011) Adsorption interaction of astatine species with quartz and gold surfaces. Radiochim Acta 99:593–600. https://doi.org/10.1524/ract.2011.1850
38. Eichler R, Aksenov NV, Belozerov AV et al (2007) Chemical characterization of element 112. Nature 447:72–75. https://doi.org/10.1038/nature05761
39. Steinegger P, Asai M, Dressler R et al (2016) Vacuum chromatography of Tl on SiO_2 at the single-atom level. J Phys Chem C 120:7122–7132. https://doi.org/10.1021/acs.jpcc.5b12033
40. Fan W, Gäggeler H (1982) Thermochromatography of Carrier-free Lead in Quartz Columns with Hydrogen and Argon as Carrier Gases. Radiochim Acta 31:95–98. https://doi.org/10.1524/ract.1982.31.12.95
41. Hänssler F, Eichler R, Gäggeler HW et al (2005) LRC PSI annual reports 2004: thermochromatographic investigation of ^{212}Pb on quartz. Paul-Scherrer-Institut, Villigen
42. Yakushev A, Lens L, Düllmann CE et al (2022) On the adsorption and reactivity of element 114, flerovium. Front Chem 10:976635. https://doi.org/10.3389/fchem.2022.976635
43. Eichler R, Aksenov NV, Albin YV et al (2010) Indication for a volatile element 114. Radiochim Acta. https://doi.org/10.1524/ract.2010.1705
44. Eichler R, Schädel M (2002) Adsorption of radon on metal surfaces: a model study for chemical investigations of elements 112 and 114. J Phys Chem B 106:5413–5420. https://doi.org/10.1021/jp015553q
45. Pershina V (2018) Reactivity of superheavy elements Cn, Nh, and Fl and their lighter homologues Hg, Tl, and Pb, respectively, with a gold surface from periodic DFT calculations. Inorg Chem 57:3948–3955. https://doi.org/10.1021/acs.inorgchem.8b00101
46. Ryzhkov A, Pershina V, Iliaš M et al (2024) Reactivity of Ts and At oxides and oxyhydrides with a gold surface from periodic DFT calculations. PCCP 26:9975–9983. https://doi.org/10.1039/d3cp05645g
47. Aksenov NV, Steinegger P, Abdullin FS et al (2017) On the volatility of nihonium (Nh, Z = 113). Eur Phys J A. https://doi.org/10.1140/epja/i2017-12348-8
48. Yakushev A, Lens L, Düllmann CE et al (2021) First study on Nihonium (Nh, element 113) chemistry at TASCA. Front Chem 9:753738. https://doi.org/10.3389/fchem.2021.753738
49. Skuja L, Hirano M, Hosono H et al (2005) Defects in oxide glasses. Phys Status Solid 2:15–24. https://doi.org/10.1002/pssc.200460102
50. Tso ST, Pask JA (1982) Reaction of fused silica with hydrogen gas. J Am Ceram Soc 65:457–460. https://doi.org/10.1111/j.1151-2916.1982.tb10514.x
51. Zhuravlev LT (2000) The surface chemistry of amorphous silica. Zhuravlev model. Colloids Surf A Physicochem Eng Asp 173(1–3):1–38. https://doi.org/10.1016/S0927-7757(00)00556-2
52. Rimola A, Costa D, Sodupe M et al (2013) Silica surface features and their role in the adsorption of biomolecules: computational modeling and experiments. Chem Rev 113:4216–4313. https://doi.org/10.1021/cr3003054
53. Chiera NM, Aksenov NV, Albin YV et al (2023) Observation of a volatile astatine hydroxide species in online gas-adsorption

thermochromatography experiments. Mol Phys. https://doi.org/10.1080/00268976.2023.2272685
54. Stickler JD, Hofstetter KJ (1974) Comparison of He3 -, He4 -, and C12 -induced nuclear reactions in heavy-mass targets at medium excitation energies. I. Experimental cross sections. Phys Rev C 9:1064–1071. https://doi.org/10.1103/PhysRevC.9.1064
55. Velmuzhov AP, Sukhanov MV, Churbanov MF et al (2018) Behavior of hydroxyl groups in quartz glass during heat treatment in the range 750–950°C. Inorg Mater 54:925–930. https://doi.org/10.1134/S0020168518090169
56. Zvára I (1985) Simulation of thermochromatographic processes by the Monte Carlo method. Radiochim Acta 38:95–102. https://doi.org/10.1524/ract.1985.38.2.95
57. Dietzel D, Yakushev A, Düllmann CE (2024) An extended monte carlo simulation code for modeling gas chromatography experiments with superheavy elements and their homologs. J Radioanal Nucl Chem. https://doi.org/10.1007/s10967-023-09290-9
58. Iliaš M, Pershina V (2024) Theoretical predictions of properties and adsorption behaviour of a superheavy element Ts and its lighter homolog At, and of their various gas-phase compounds, on hydroxylated quartz surfaces from periodic DFT calculations. Mol Phys. https://doi.org/10.1080/00268976.2024.2363408
59. Nishinaka I, Hashimoto K (2021) Separation of astatine from irradiated lead targets based on dry distillation in a glass test tube. J Radioanal Nucl Chem 327:869–875. https://doi.org/10.1007/s10967-020-07546-2
60. Nishinaka I, Washiyama K, Hashimoto K (2021) Adsorption temperature of volatile astatine species formed via dry distillation in a glass tube. J Radioanal Nucl Chem 329:1459–1465. https://doi.org/10.1007/s10967-021-07879-6
61. Huber F, Berwanger J, Polesya S et al (2019) Chemical bond formation showing a transition from physisorption to chemisorption. Science 366:235–238. https://doi.org/10.1126/science.aay3444
62. Borodin D, Rahinov I, Shirhatti PR et al (2020) Following the microscopic pathway to adsorption through chemisorption and physisorption wells. Science 369:1461–1465. https://doi.org/10.1126/science.abc9581
63. Steinegger P, Asai M, Dressler R et al (2016) Vacuum chromatography of Tl on SiO_2 at the single-atom level. J Phys Chem C 120:7122–7132. https://doi.org/10.1021/acs.jpcc.5b12033